Comparison of traveltime computation and ray tracing methods

Bernard Law and Daniel Trad

ABSTRACT

Travel times and ray paths of the propagation of seismic body wave in heterogenous media are used in seismic tomography, imaging and inversion processes. In this study, we review the seismic ray theory, basic principles of the fast marching, wavefront construction and paraxial method. We analyze their differences and similarities to investigate the effectiveness of these methods in refraction tomography and seismic imaging. We compare the travel times from these method to a finite difference synthetic shot record of the Marmousi model and find travel time from all three methods are accurate except at area where rays diverge. We also used the travel time from the fast marching method in the refraction tomography processing of the Hussar 2D dataset. The CDP stack from the refraction tomography processing is more coherent and better resolved than the CDP stack with datum static correction only.

INTRODUCTION

Traveltime computation and ray tracing are important steps in seismic modeling, migration, tomographic inversion, velocity model building and many other applications. Core principles of most traveltime and ray tracing algorithms are derived from the seismic ray theory.

High frequency approximation of the solution of elastodynamic equation leads to solutions in different forms. For kinematic ray tracing, the solution leads to the eikonal equation and the ray equations. The high frequency approximation requires the velocity of the media to vary smoothly. Vidale (1988,1990) presented a grid based traveltime computation scheme that solves the eikonal equation by finite difference approximation. Vidale's work leads to subsequent studies and developments by Qin (1992), Sethian and Popovici (1999) and other authors, and resulted in more robust algorithms that can better handle rapid velocity variations. Results of these algorithms are traveltime from source to regularly spaced grid points. Vidale (1988) proposed the construction of the ray paths by tracing the steepest traveltime gradient from the receiver back to the source. Matsuoka (1992) presented a ray path reciprocity method that traces the minimum time of summed shot and receiver traveltime tables. Alternate to grid based traveltime computation scheme are kinematic and dynamic ray tracing (Cerveny and Hron,1980; Beydoun and Keho,1987), and wavefront construction method (Vinje,1993). These methods involve tracing the ray path by computing the solutions to the ray equations at each ray step. Some geophysical applications such as Kirchhoff migration requires only traveltime from a source or receiver to a subsurface point; while other applications such as refraction tomography requires both first arrival time and ray path between a source and receiver. The purpose of this study is to review the basic principles of the fast marching method, paraxial method and wavefront construction method, and to evaluate their accuracy and effectiveness when applied in refraction tomography and depth imaging.

Seismic ray method and eikonal equation

Seismic ray method is based on asymptotic high frequency solution of the elastodynamic equation. For an inhomogeneous, isotropic and perfectly elastic medium described by Lam**é** parameters $\boldsymbol{\lambda, \mu}$ and density $\boldsymbol{\rho}$, the elastodynamic equation and the stress-strain relationship can be written as:

$$\sigma_{ij,j} + f_i = \rho \ddot{u}_i \quad (1)$$

$$\sigma_{ij} = c_{ijkl} u_{k,l} \quad (2)$$

$$c_{ijkl} = \lambda \delta_{ij} \delta_{kl} + \mu\left(\delta_{ik}\delta_{jl} + \delta_{il}\delta_{jk}\right) \quad (3)$$

where $\boldsymbol{f_i}$ is the body force, $\boldsymbol{\sigma_{ij}}$ is the stress tensor, $\boldsymbol{u}$ is the displacement vector, $\boldsymbol{c_{ijkl}}$ is elastic constant tensor and satisfies the following symmetry relationship:

$$\boldsymbol{c_{ijkl} = c_{jikl} = c_{ijlk} = c_{klij}}$$

This symmetry relationship reduces $\boldsymbol{c_{ijkl}}$ from 81 components to 21 components. The components of $\boldsymbol{c_{ijkl}}$ are often expressed in Voigt notation with two indices instead of four. For isotropic media, $\boldsymbol{c_{ijkl}}$ in Voigt notation is:

$$\begin{bmatrix} \lambda+2\mu & \lambda & \lambda & 0 & 0 & 0 \\ \lambda & \lambda+2\mu & \lambda & 0 & 0 & 0 \\ \lambda & \lambda & \lambda+2\mu & 0 & 0 & 0 \\ 0 & 0 & 0 & \mu & 0 & 0 \\ 0 & 0 & 0 & 0 & \mu & 0 \\ 0 & 0 & 0 & 0 & 0 & \mu \end{bmatrix}$$

$\boldsymbol{\delta}$ is Kronecker delta, $\boldsymbol{\delta_{ij} = 1 \quad for\ i = j, \quad \delta_{ij} = 0 \quad for\ i \neq j}$

The measurement units for these quantities are: $\boldsymbol{\sigma_{ij}}$ in pascals or $\boldsymbol{kg\ m^{-1}s^{-2}}$, $\boldsymbol{f_i}$ **in** $\boldsymbol{N\ m^{-3}}$ or $\boldsymbol{kg\ m^{-2}s^{-2}}$, $\boldsymbol{\rho}$ **in** $\boldsymbol{kg\ m^{-3}}$ **and** $\boldsymbol{u_i}$ **in** $\boldsymbol{m}$.
Equation (1) is the elastodynamic equation, also known as the equation of motion. Equation (2) is the Hooke's Law for a perfectly elastic medium. Equation (3) relates the elastic constant tensor to the Lam**é** parameters for an isotropic medium.

General harmonic wave solution to equation (1) is in the form of:

$$u_i(\vec{x}) = A_i(\vec{x}) \exp\{-i\omega[t - T(\vec{x})]\} \quad (4)$$

where $\boldsymbol{\omega}$ is the radial frequency, $\boldsymbol{T(\vec{x})\ and\ |A\ (\vec{x})|}$ are the traveltime and amplitude of the body avew at $\vec{x}$.

Substitute (2) and (4) into (1), set $\boldsymbol{f_i}$=0, take the derivatives of $\boldsymbol{u_i}$ and equating the real parts gives:

$$\left(c_{ijkl,j}A_{k,j} + c_{ijkl}\,A_{k,lj}\right)\omega^{-2} - c_{ijkl}\,T_{,j}T_{,l}A_k = -\rho\delta_{ik}A_k \quad (5)$$

For large $\boldsymbol{\omega}$ (high frequency approximation), we drop $\boldsymbol{\left(c_{ijkl,j}A_{k,j} + c_{ijkl}\,A_{k,lj}\right)\omega^{-2}}$ and obtain:

$$c_{ijkl}\,T_{,j}T_{,l}A_k = \rho\delta_{ik}A_k \qquad (6)$$

Defining $B_{ik} = c_{ijkl}\,T_{,j}T_{,l}$ gives:

$$(B_{ik} - \rho\,\delta_{ik})A_k = 0 \quad \text{or in matrix form } [\,\mathrm{B} - \rho\mathrm{I}]\mathrm{A} = 0 \qquad (7)$$

Equation (7) is an eigenvalue problem and its solution is the eikonal equation: $\det[\,\mathrm{B} - \rho\mathrm{I}] = 0$

Evaluating $\det[\,\mathrm{B} - \rho\mathrm{I}] = 0$, we obtain:

$$-\rho^3 + (T_{,k}T_{,k})\rho^2[(\lambda + 2\mu) + 2\mu] - (T_{,k}T_{,k})^2\rho\mu[2(\lambda + 2\mu) + \mu] + (T_{,k}T_{,k})^3\mu^2(\lambda + 2\mu) = 0 \qquad (8)$$

Defining P and S wave velocities: $\alpha = \sqrt{\frac{\lambda+2\mu}{\rho}}$ and $\beta = \sqrt{\frac{\mu}{\rho}}$ reduces equations (8) to $\left(\boldsymbol{T_{,k}T_{,k}} - \frac{\mathbf{1}}{\boldsymbol{\alpha^2}}\right)\left(\boldsymbol{T_{,k}T_{,k}} - \frac{\mathbf{1}}{\boldsymbol{\beta^2}}\right) = \mathbf{0}$ (9)

Conditions that satisfy equation (9) are:

$$T_{,k}T_{,k} = \frac{1}{\alpha^2} \quad \text{and} \quad T_{,k}T_{,k} = \frac{1}{\beta^2}$$

This can be written as the following and is referred to as the eikonal equation:

$$\left(\vec{\nabla}T\right)^2 = \frac{1}{c^2}$$

or $$\left(\frac{\partial T}{\partial x}\right)^2 + \left(\frac{\partial T}{\partial y}\right)^2 + \left(\frac{\partial T}{\partial z}\right)^2 = \frac{1}{c^2} \qquad (10)$$

where $\boldsymbol{\vec{\nabla}T}$ is the slowness vector and c is $\boldsymbol{\alpha}$ $\boldsymbol{or}$ $\boldsymbol{\beta}$.

Solving equation (10) provides the traveltime T(x,y,z).

Ray equations

To trace the position of a ray, we have to define some properties of rays and wavefronts (Figure 1) and to express their relationships as a set of ray equations. Wavefronts are defined by the surfaces T(x,y,z)=constant. Slowness vector $\vec{\mathbf{q}}$ **equals** $\boldsymbol{\vec{\nabla}T}$ and is tangential to the ray and normal to the wavefronts.

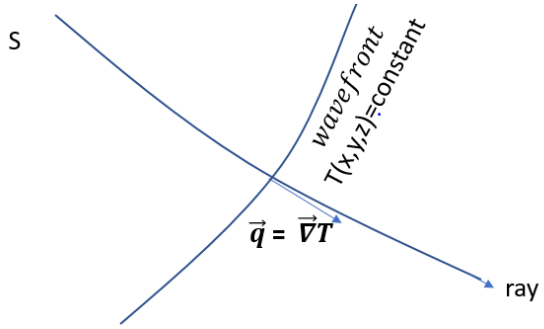

Figure 1.Relationship between ray and wavefront

From equation (10), we have $|\,\boldsymbol{c\,\vec{\nabla}T}| = \mathbf{1}$ being a unit vector normal to the wavefront. Therefore, ray can be defined by a set of normal equations in the form of:

$$\frac{d\vec{x}}{ds} = c\,\vec{\nabla}T = c\,\vec{q}$$

$$or \qquad \frac{dx_i}{ds} = cq_i, \quad i = 1,2,3 \qquad (11)$$

where $\frac{d\vec{x}}{ds}$ is a unit vector tangential to the ray.

From $\vec{q} = \vec{\nabla}T$, we can obtain $\frac{d\vec{q}}{ds} = \frac{d}{ds}\vec{\nabla}T$ (12)

Substitute (11) into (12), we obtain the ray equations for the slowness vectors:

$$\frac{d\vec{q}}{ds} = \frac{d}{ds}\left[\frac{1}{c}\frac{d\vec{x}}{ds}\right] = \vec{\nabla}\left[\frac{1}{c}\right] \quad (13)$$

Ray equations can also be expressed in terms of T instead of arc length, s :

$$\frac{d\vec{x}}{dT} = c^2\,\vec{q} \quad (14)$$

and

$$\frac{d\vec{q}}{dT} = c\,\vec{\nabla}\left[\frac{1}{c}\right] \quad (15)$$

These equations form the kinematic ray tracing system. Solution of equation (12) or (14) represents the trajectory $\vec{x}$, while solution of equation (13) or (15) represents the slowness vector $\vec{q}$ along the ray as function of arc length or time.

Finite difference solution to the eikonal equation and grid based method

Grid based travel time computation algorithms use the eikonal equation (10) to solve for T(x,y,z). Vidale (1988) presented a method that uses first order finite difference approximation scheme to propagate geometric rays from three corners to the fourth corner of a square grid as shown in figure 2. Equation (16) and (17) are the average finite difference approximation of $\frac{\partial T}{\partial x}$ and $\frac{\partial T}{\partial z}$ respectively.

$$\left(\frac{\partial T}{\partial x}\right)^2 + \left(\frac{\partial T}{\partial z}\right)^2 = s(x,z)^2 \quad (15)$$

$$\frac{\partial T}{\partial x} = \frac{1}{2h}\,(t_0 + t_2 - t_1 - t_3) \quad (16)$$

$$\frac{\partial T}{\partial z} = \frac{1}{2h}\,(t_0 + t_1 - t_2 - t_3) \quad (17)$$

Substitutes equations (16) and (17) into equation (15):

$$t_3 = t_0 + \sqrt{2(h\bar{s})^2 - (t_2 - t_1)^2} \quad (18)$$

Where: s(x,z) is the slowness,
t_0, t_1 and t_2 are computed travel times,
t_3 is travel time to be computed

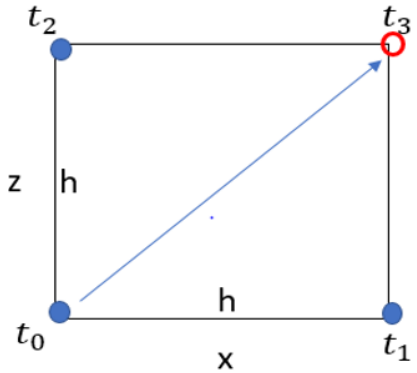

Figure 2. Using t_0, t_1 and t_2 to compute t_3

The procedure starts at the source and expands outward as square rings (Figure 3). Points on the square ring are sorted from minimum traveltime to maximum traveltime, and the new traveltime is computed starting from the point with minimum travel time.

Expanding wavefront method

Qin (1992) showed that the expanding square strategy is not appropriate for model with moderate to large velocity contrast and can lead to negative value in the square root term in equation (18). Qin proposed an expanding wavefront method that can preserve the causality by expanding the wavefront only at points adjacent to the point with global minimum traveltime (shown as double circle in Figure 4). This method ensures a ray associated with a point to be considered is completely timed up to that point. However, it is computationally expensive at $\mathbf{0}(\mathbf{N^3})$ algebraic operations, because sorting is required to establish the new global minimum after each wavefront point is added.

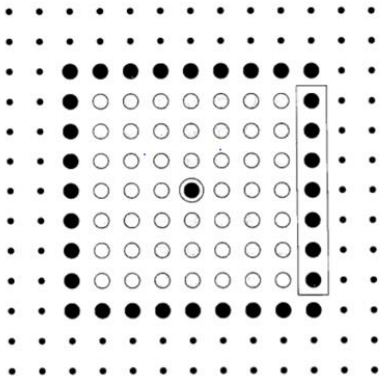

Figure 3. Double circle shows the source point. Empty circles are timed locations. Filled circles are locations to be timed. Large filled circles are the square wavefront to be timed. Points on each edge are timed from location of minimum time to maximum time. (Adapted from Vidale 1988)

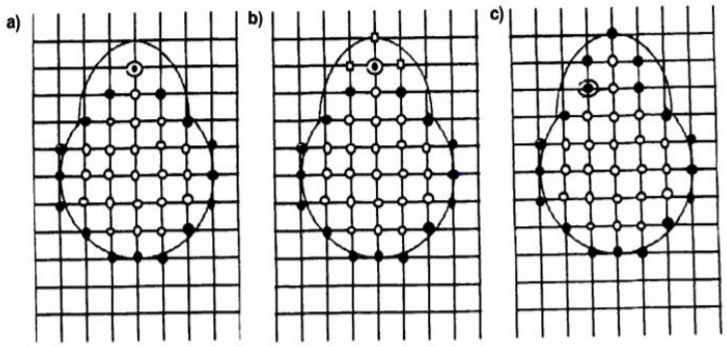

Figure 4. (a) Filled circles mark the outer cicrumference of timed locations. Double circle shows the location of minimum time on current timed wavefront. (b) new locations to be timed (empty circles next to double circle). (c) New locations in (b) are timed and new minimum time of current wavefront is marked as double circle. (Adapted from Qin 1992)

Fast marching method

Sethian and Popovici (1999) showed that propagating a triangular wavefront with unit speed using central difference approximation to the travel time gradient results in instabilities at the bend of the triangular wavefront. Rapid changes in velocity can result in similar instabilities. These instabilities are resolved by applying entropy-satisfying upwind differences schemes introduced by Osher and Sethian (1988) :

$$\Psi_x^2 \approx [\max(D_i^{-x}\,\Psi, 0)^2 + \min(D_i^{+x}\,\Psi, 0)^2\,] \qquad (19)$$

A more convenient upwind scheme from Rouy and Tourin (1992) is used in Sethian and Popovici's fast marching method:

$$\Psi_x^2 \approx \max(D_i^{-x}\,\Psi, -D_i^{+x}\,\Psi, 0)^2 \quad (20)$$

where D^- and D^+ are backward and forward difference operators :

$$D_i^{-x}\Psi = \left(\frac{\Psi_i - \Psi_{i-1}}{h}\right)$$
$$D_i^{+x}\Psi = \left(\frac{\Psi_{i+1} - \Psi_i}{h}\right)$$

Ψ_i is the value of Ψ at grid point i and h is the grid spacing

The upwind scheme chooses grid points in terms of the direction of the flow of information. Sethian and Popovici (1999) express the eikonal equation as the following and apply the upwind finite difference scheme:

$$|\nabla t(x, y, z)| = s(x, y, z) \quad (21)$$

$$|\nabla t| \approx \left[\max\left(D_{ijk}^{-x}\,t, -D_{ijk}^{+x}\,t, 0\right)^2 + \max\left(D_{ijk}^{-y}\,t, -D_{ijk}^{+y}\,t, 0\right)^2 + \max\left(D_{ijk}^{-z}\,t, -D_{ijk}^{+z}\,t, 0\right)^2\right]^{\frac{1}{2}} = S_{ijk} \quad (22)$$

where $\mathbf{S_{ijk}}$ **is the slowness at grid point**$(\mathbf{i}, \mathbf{j}, \mathbf{k})$.

To solve for $\boldsymbol{t_{ijk}}$,we expand equation (22) to a quadratic equation in the form of $\boldsymbol{at^2 + bt + c = 0}$

$\boldsymbol{t_{ijk}}$ can now be solved explicitly as the root to a quadratic equation using $\boldsymbol{t = \frac{-b \pm \sqrt{b^2 - 4ac}}{2a}}$

The fast march algorithm also stores the traveltime values on a heap with the minimum time on top of the heap to reduce the sorting effort. This reduces the computationally cost to $\mathbf{0}(\mathbf{NlogN})$ algebraic operations.

The fast marching algorithm is outlined in the following steps:

First compute traveltimes at locations around source point and tag these locations as ACCEPTED. Then tag as CLOSE all points one grid point away. Finally, tag as FAR all other grid points.

1) Begin Loop: Let TRIAL be the point in CLOSE with the smallest traveltime
2) Add the point TRIAL to ACCEPTED; remove it from CLOSE.
3) Tag as CLOSE all neighbors of TRIAL that are not ACCEPTED. If the neighbor is in FAR remove it from that list and add it to the set CLOSE.
4) Recompute traveltimes at all neighbor according to equation (22).
5) Return to 1.

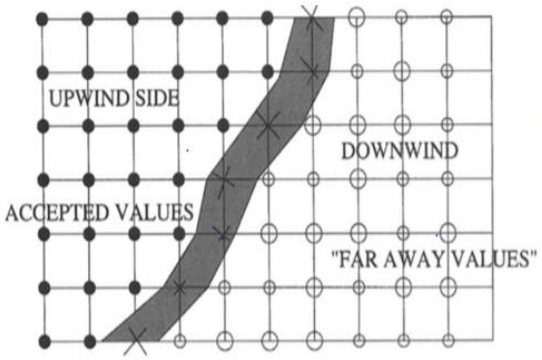

Figure 5. Fast marching scheme. Filled circles are timed locations. X's are CLOSE locations to be tested for minimum time. Empty circles are FAR locations have not been times.

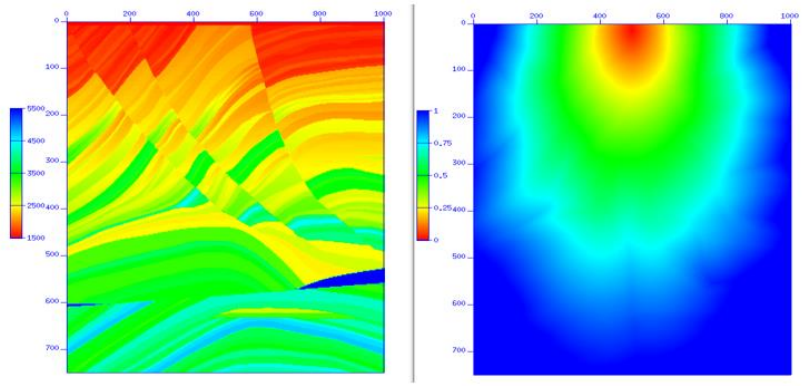

Figure 6. Input velocity model and minimum traveltime from fast marching method.

Ray Shooting method

Ray shooting method (Figure 7) shoots a series of rays through the medium with starting vertical angle $\boldsymbol{\theta_i}$ and horizontal angle $\boldsymbol{\phi_i}$, and uses the ray equations to computes the trajectory of the ray paths. Travel times along the ray paths are then computed by integrating through the velocity model. Finally, the computed travel times are mapped to the subsurface grid by interpolation.

Initial value of equations (11) for isotropic medium is:

$$\frac{d\vec{x}}{ds} = (sin\theta_i\, cos_i\phi, sin\theta_i\, sin\phi_i, cos\theta_i) \qquad (23)$$

The initial value for the ray parameter for isotropic medium is:

$$\vec{\boldsymbol{q}} = \frac{\mathbf{1}}{\boldsymbol{c(Xs,Ys,Zs)}} \frac{\boldsymbol{d\vec{x}}}{\boldsymbol{ds}} \qquad (24)$$

Trajectory $\vec{\boldsymbol{x}}$ of the ray is computed with the following steps:

1: Solve ODE (11) for $\vec{\boldsymbol{x}}$

2: Solve ODE (13) for $\vec{\boldsymbol{q}}$.

Repeat step 1 and 2 for all depth steps.

Repeat for all starting angles $\boldsymbol{\theta_i}$ $\boldsymbol{and}$ $\boldsymbol{\phi_i}$

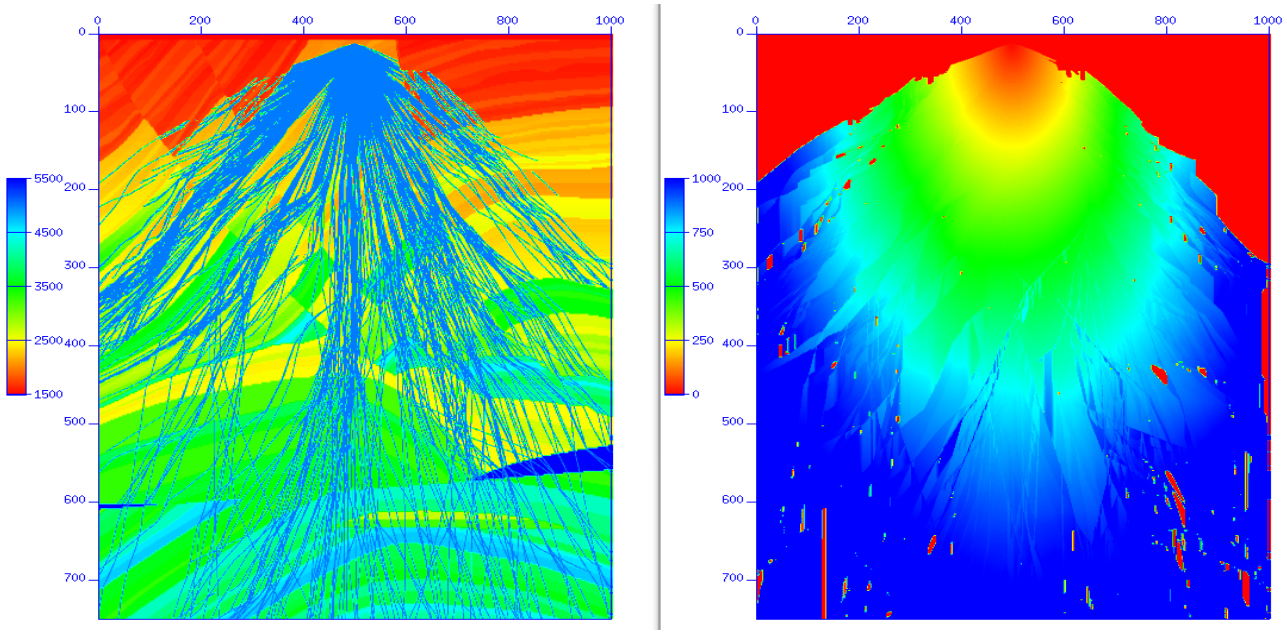

(a) (b)

Figure 7. a) Input velocity model and rays, b) interpolated traveltime.

Wavefront Construction

Wavefront construction (WFC) is a natural extension of the ray shooting method. WFC uses localized ray tracing to construct wavefront of constant traveltimes. Amplitude of rays can be computed from ratio of cross-sectional area of rays of adjacent wavefronts. The initial wavefront is constructed by shooting a series of short ray segments of equal time step from the source. The end points of the ray segments on the wavefront are then propagated for another time step to construct a new wavefront. Coordinates of position and components of slowness vector of the ray segments are computed using same procedure as the ray shooting method. When the wavefront crosses an interface with rapid velocity changes, the ray segments diverge and create a gap or shadow zone. The ray segments can also cross over and create caustics or multi-values (Figure 8a). To address the problem of shadow zones and to ensure sufficient ray density, additional ray segments can be interpolated (Figure 8b). For minimum traveltime ray tracing, caustics can be removed (Figure 8c). Figure 8d shows gridded minimum traveltime after caustics are removed.

In this example, upgoing rays are disabled for depth imaging. However, if caustics are to be removed, upgoing rays can be enabled for refraction ray tracing.

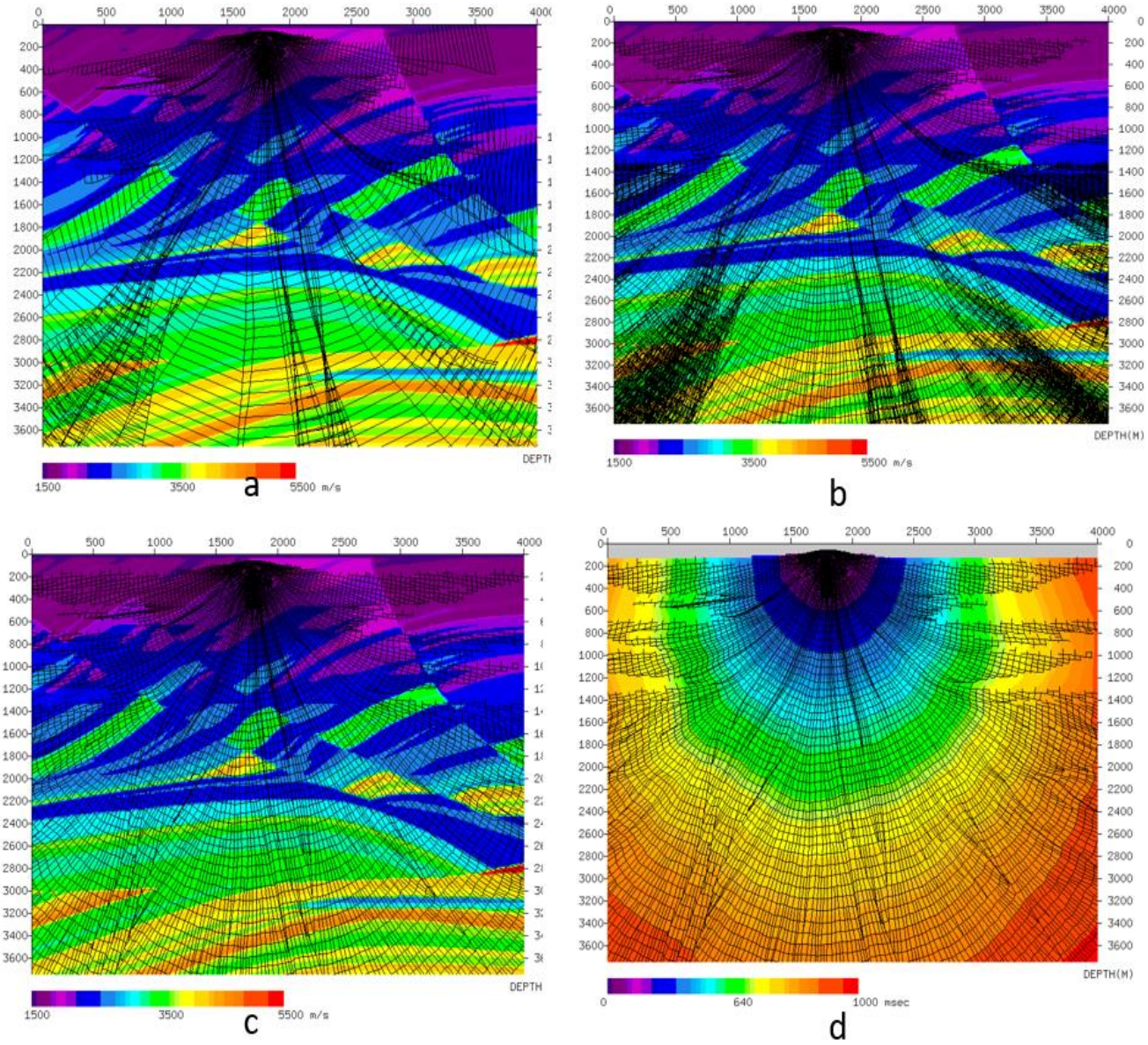

Figure 8. a) Wavefronts without interpolation, b) wavefronts with third-order interpolation along wavefronts, c) wavefronts with caustics removed, d) travel time gridded from wavefronts.

Paraxial method

Paraxial method is a dynamic ray tracing method in ray coordinate system (γ_1, γ_2, u) or ray-centered coordinate system (q_1, q_2, q_3). The following discussion refers to the ray coordinate system shown in figure 9a. Paraxial rays are rays in the vicinity of a central ray (Figure 9b). γ_1 and γ_2 are ray parameters. They can be take-off angles i_0 and ϕ_0, or they can be components of slowness vector. They specify the initial direction of the ray in isotropic media. For anisotropic media, they specify the initial direction of the

slowness vector. The third ray parameter u is a monotonically changing parameter along the ray. It can be arc length s or travel time T.

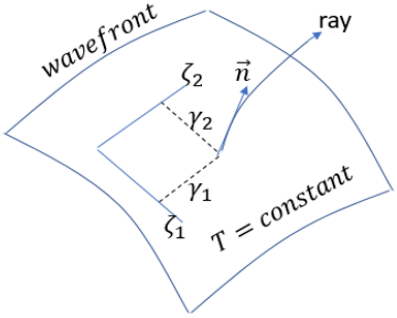

(a)

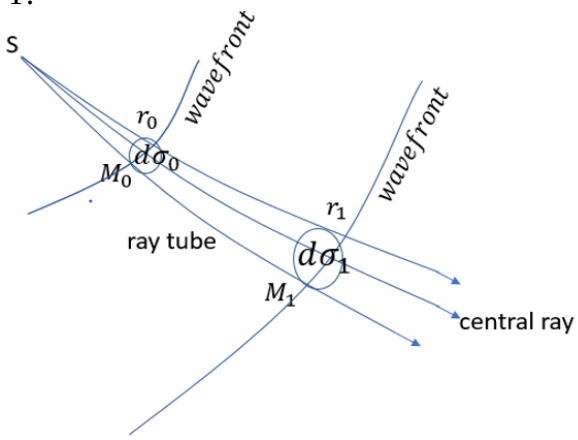

(b)

Figure 9. a) ray coordinates ζ_1, ζ_2; ray parameters γ_1, γ_2 and wavefront T.

9. b) paraxial rays are rays in the vicinity of of the central ray. $d\sigma_0$ is the cross sectional area of the paraxial ray, r_0 is radius of curvature of the wavefront at M_0. Similarly, for $d\sigma_1 and\, r_1$.

Paraxial rays can have different properties than the central ray. These properties can be travel times or amplitude. Paraxial method determines these properties by differentiating the ray equations with respect to $\gamma_1\ and\ \gamma_2$. If we choose u=s, we can start with ray equations in the form of:

$$\frac{dx_i}{ds} = c\, p_i \tag{26}$$

$$\frac{dp_i}{ds} = \frac{d}{dx_i}\left[\frac{1}{c}\right] \tag{27}$$

Dynamic ray tracing equations

We define:

$$Q_i \equiv \frac{\partial x_i}{\partial \gamma}, P_i \equiv \frac{\partial p_i}{\partial \gamma} \tag{28}$$

To derive the dynamic ray tracing equations, we take the derivatives of (26) and (27):

$$\frac{\partial}{\partial \gamma}\frac{dx_i}{ds} = \frac{d}{ds}\frac{\partial x_i}{\partial \gamma} = \frac{dQ_i}{ds} = \frac{\partial c}{\partial \gamma}\, p_i + cP_i$$

$$\frac{dQ_i}{ds} = \frac{\partial c}{\partial x_k}\frac{\partial x_k}{\partial \gamma} p_i + cP_i = c_{,k}\, Q_k p_i + cP_i \tag{29}$$

$$\frac{\partial}{\partial \gamma}\frac{dxp_i}{ds} = \frac{d}{ds}\frac{\partial p_i}{\partial \gamma} = \frac{dP_i}{ds} = \frac{\partial}{\partial \gamma}\left(\frac{d}{dx_i}\left[\frac{1}{c}\right]\right)$$

$$\frac{dP_i}{ds} = \left(\frac{\partial}{\partial x_k}\frac{\partial}{\partial x_i}\left(\frac{1}{c}\right)\right)\frac{\partial x_k}{\partial \gamma} = \frac{\partial^2}{\partial x_i \partial x_k}\left(\frac{1}{c}\right) Q_k \qquad (30)$$

Equation (29) and (30) are dynamic ray tracing equations and are used to compute $\boldsymbol{Q_i}$ **and** $\boldsymbol{P_i}$ for the central ray.

Paraxial ray tracing equations

We define $\boldsymbol{\delta x_i}$ ***and*** $\boldsymbol{\delta p_i}$ as parameters that connect a paraxial ray to the central ray using the following approximation:

$$\delta x_i \approx \frac{\partial x_i}{\partial \gamma} d\gamma = Q_i \, d\gamma \qquad (31)$$

$$\delta p_i \approx \frac{\partial p_i}{\partial \gamma} d\gamma = P_i \, d\gamma \qquad (32)$$

Multiplying equation (29) and (30) with $\delta\gamma$ and apply equation (31) and (32) yields:

$$\frac{dQ_i}{ds}\,\delta\gamma = c_{,k}\, Q_k p_i \delta\gamma + cP_i\delta\gamma$$

$$\frac{d}{ds}\delta x_i = c_{,k}\,\delta x_k\, p_i + c\delta p_i \qquad (33)$$

$$\frac{dP_i}{ds}\,\delta\gamma = \frac{\partial^2}{\partial x_i \partial x_k}\left(\frac{1}{c}\right) Q_k \delta\gamma$$

$$\frac{d}{ds}\delta p_i = \frac{\partial^2}{\partial x_i \partial x_k}\left(\frac{1}{c}\right)\delta x_k = \left(\frac{2c_{,i}c_{,k}}{c^3} - \frac{c_{,ik}}{c^2}\right)\delta x_k \qquad (34)$$

Equation (33) and (34) are paraxial ray tracing equations and are used to compute $\boldsymbol{\delta x_i}$ ***and*** $\boldsymbol{\delta p_i}$ for paraxial ray from $\boldsymbol{c, \vec{\nabla} c}$ ***and*** $\boldsymbol{\vec{p}}$.

Geometrical spreading factor

Geometrical spreading can be computed from the ratio of cross sectional areas. Equation (31) shows that cross sectional area of paraxial ray can be computed directly from $\boldsymbol{Q_1}$ ***and*** $\boldsymbol{Q_2}$ and the ray parameters $\boldsymbol{\gamma_1}$ ***and*** $\boldsymbol{\gamma_2}$:

$$d\sigma = \left|\frac{\partial \vec{x}}{\partial \gamma_1} \mathrm{x} \frac{\partial \vec{x}}{\partial \gamma_2}\right| d\gamma_1 d\gamma_2 = Q_1 Q_2 d\gamma_1 d\gamma_2 \qquad (35)$$

Paraxial ray traveltimes

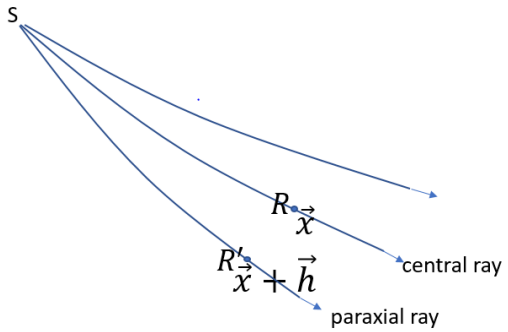

Figure 10. Paraxial ray and traveltime

As shown in figure 10, a point R is at $\vec{\boldsymbol{x}}$ on the central ray and a point R' is at $\vec{\boldsymbol{x}}+\vec{\boldsymbol{h}}$ on a nearby ray. Using 3D Taylor series to relate R and R', we obtain:

$$T\left(\vec{x}+\vec{h}\right)=T(\vec{x})+T_{,j}\ (\vec{x})h_j+\frac{1}{2}T_{,jk}\,(\vec{x})h_jh_k \qquad (36)$$

Where $T(\vec{x})$ is travel time at R,

$T_{,j}$ is the first derivative of traveltime and equals p_j

$T_{,jk}$ is the second derivative of traveltime and can be computed from:

$$T_{,jk}=\frac{\partial p_j}{\partial x_k}=\frac{\partial p_j}{\partial \gamma_n}\frac{\partial \gamma_n}{\partial x_k}=P_{jn}Q_{nk}^{-1} \qquad (37)$$

where $Q_{nk}^{-1}=\frac{\partial \gamma_n}{\partial x_k}$

Or in matrix form: $T_{,jk}=\mathrm{T}=\mathrm{PQ}^{-1}$ (38)

The paraxial ray tracing algorithm is outlined in the following steps:

1) Shoot a ray through the medium with starting vertical angle $\boldsymbol{\theta_i}$ and horizontal angle $\boldsymbol{\phi_i}$
2) Solve ODE 26 for displacement $\boldsymbol{x_i}$ for the central ray
3) Solve ODE 27 for slowness vector $\boldsymbol{p_i}$ for the central ray
4) Solve ODE 29 and 30 for $\boldsymbol{P_i}$ $\boldsymbol{and}$ $\boldsymbol{Q_i}$
5) Use equation 37 to compute $\boldsymbol{T_{,jk}}$
6) Use equation 36 to compute paraxial travel time for paraxial rays near the central ray

Repeat step 1 to 6 for all starting angle $\boldsymbol{\theta_i}$ and horizontal angle $\boldsymbol{\phi_i}$

Comparisons of travel times from ray tracing methods

To verify and compare the accuracy of the travel times computed from WFC (Figure 11a), fast marching and paraxial method (Figure 11b), we use the Marmousi model with the source placed at the depth of 2500m and compute the travel times from these three methods. A second order finite difference shot record was created using Seismic Unix module sufdmod2. Travel times at the surface are plotted on the shot record with travel times from WFC plotted in red, fast marching plotted in blue and paraxial method plotted in yellow (Figure 12). As shown in figure 12, the travel times at the surface from WFC and fast marching are almost identical. Travel times at the surface from paraxial method that uses shortest ray path agree with the other two methods at most locations except at locations where rays diverge. This test demonstrated all three methods result in very similar travel times that agree with the finite difference shot record. Both WFC and fast marching method produce smooth and stable minimum travel times. Rays in paraxial method may diverge and create large gaps that can result in inaccurate travel times.

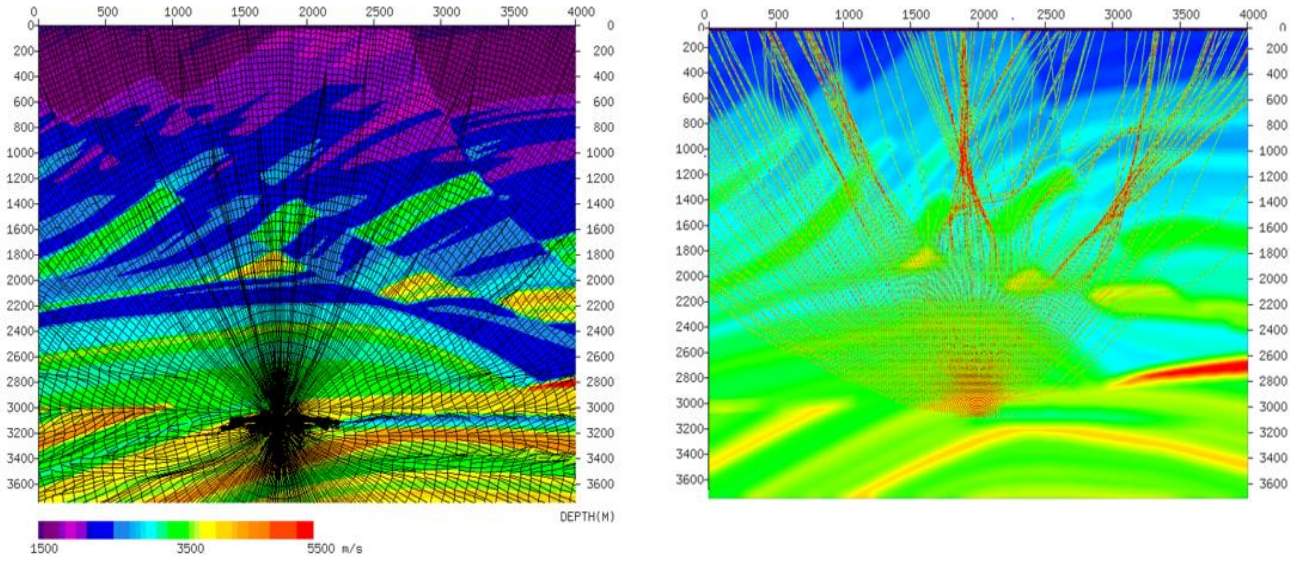

(a) (b)

Figure 11. a) Ray paths and wavefronts from WFC method, b) Ray paths from Paraxial method.

WFC and paraxial methods also show that rays can cross-over in area with complex velocity structure. These cross-over ray paths result in multi-arrivals at the same grid point. Furthermore, WFC computes geometric spreading amplitude using cross-sectional area ratio at the starting and end points of ray segment and paraxial method computes amplitude from dynamic ray tracing equations. Therefore, WFC and paraxial method can be used when multi-arrivals or different branches of traveltime including most energetic arrivals is desirable.

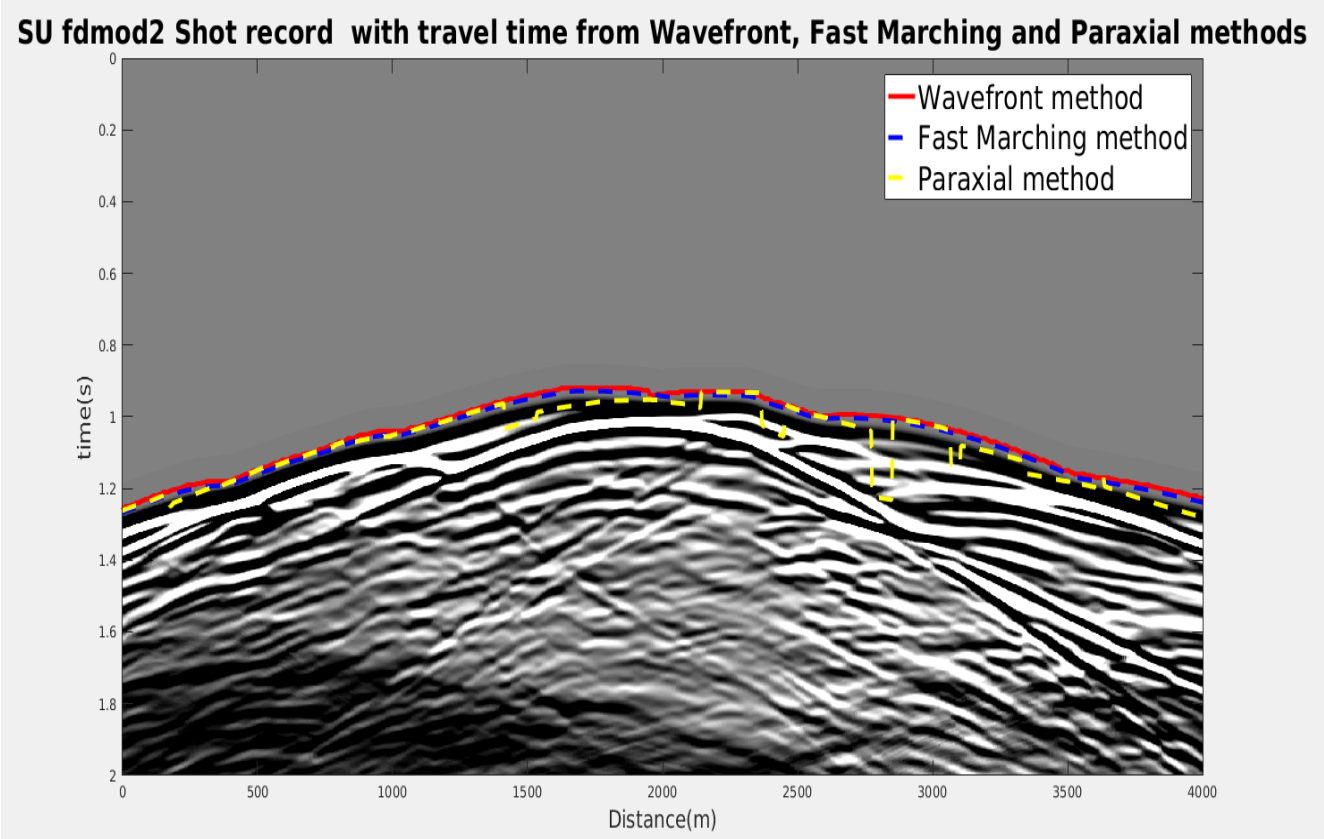

Figure 12. Finite difference synthetic shot record with first arrival times from WFC, fast marching and paraxial method

Summary of ray tracing methods

Fast marching method:

- Advantages
  - Unconditionally stable
  - Can handle turning rays. Does not have shadow zone problem.
  - Computes first arrival time for every grid point without interpolation.
  - Excellent algorithm for refraction tomography

- Disadvantages
  - Does not compute ray paths directly. Alternate computation algorithms using steepest travel time gradient or minimum time can be unstable.
  - Does not compute multi-arrivals.
  - Does not compute amplitude.
  - Can be slow for large output grid.

Wavefront Construction method:

- Advantages
  - Stable if appropriate velocity smoothing parameter is used; however, accuracy can decrease with increasing smoothing
  - Can handle turning rays. Does not have shadow zone problem.
  - Can compute multi-arrivals and amplitude
  - Can be faster than fast marching method, if larger step size is used.
  - Good algorithm for refraction tomography as well as depth imaging

- Disadvantages
  - Ray paths from interpolated ray segments may not be accurate enough for tomographic inversion.

Paraxial method:

- Advantages
  - Fast and accurate.
  - More accurate travel time interpolation in the vicinity of the central ray than classical ray shooting method.
  - Can compute multi-arrivals and amplitude
  - Good algorithm for depth imaging

- Disadvantages
  - Cannot handle turning ray. Not suitable for refraction tomography
  - Can have problem with ray path divergence and shadow zone in areas with complex structure.

Ray shooting method:

- Advantages
  - Fast and accurate.
  - Can compute multi-arrivals
  - Good algorithm for depth imaging

- Disadvantages
  - Cannot handle turning ray. Not suitable for refraction tomography
  - Travel time interpolation is not as accurate as paraxial method in the vicinity of the central ray
  - Does not compute amplitude
  - Can have problem with ray path divergence and shadow zone in areas with complex structure.

Application of ray tracing methods in depth imaging

All methods tested show similar accuracy; while WFC and the paraxial method are capable of computing multi-values traveltimes. This poses a challenge in determining which arrival times to use as well as storage and computational resources in retrieving these values. However, when minimum time and shortest path is not the optimal approach, multi-values capability of WFC and paraxial method can improve the imaging result.

We did not perform comprehensive analysis of the effects of these ray tracing methods in depth imaging. However, based on the observed geometry of the ray paths in our tests using the Marmousi model; we believe proper application of the multi-arrivals, amplitude and ray path distance information from WFC and paraxial method can have significant impact on the quality of the final depth image.

Application of ray tracing methods in refraction tomography

Refraction tomography involves forward modelling of first arrival times and using the differences between the modelled times and the actual first arrival time picks to update the velocity model along the ray path. Ray shooting method and paraxial method are not suitable for ray tracing refraction ray paths because of their inability to handle up turning rays. Both WFC and fast marching method can handle up turning rays; therefore, they are more suitable for refraction tomography. We used the fast marching method for forward modelling in refraction tomography and apply the refraction tomography process to the Hussar 2D line acquired in 2011 by CREWES of the University of Calgary. We compared the CDP stack with the tomographic statics correction to the CDP stack with GLI (Hampson and Russel 1984) weathering statics correction. GLI is one of the delay time methods and has found great success when the near surface can be approximated by layers with distinct difference in velocity, but has problem with gradational velocity changes and rough topography.

A velocity model with constant velocity gradient between layers and with the depth of the layer boundaries following the recording surface as shown in figure 13a is used as the starting model. Figure 13b shows the updated velocity model and refraction ray paths for shot location 417 after 10 iterations. Shown in figure 14 is the comparison of modeled refraction arrival times and the actual first arrival picks before and after tomographic inversion for shot location 417 as well as the RMS error for all time picks after each iteration. Figure 14b shows that modeled refraction arrival times from the final velocity model match the actual first arrival picks.

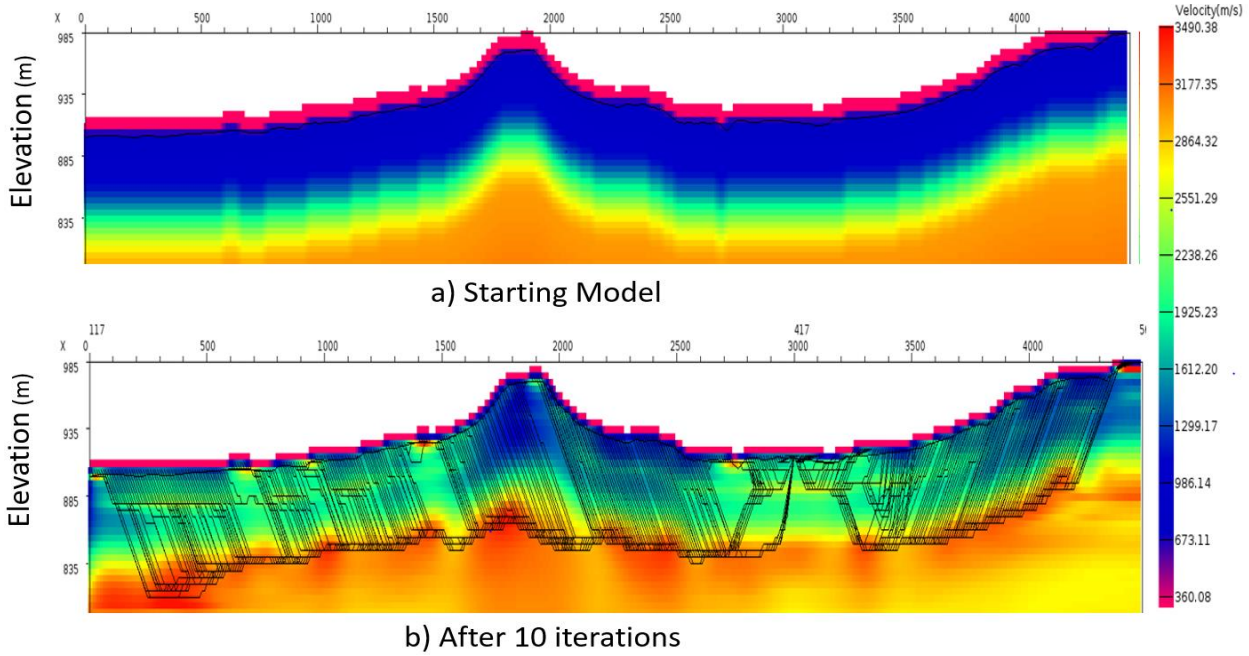

Figure 13. a) Starting model for tomographic inversion. 13b) Velocity model after 10 iterations using traveltimes from fast marching method. Ray paths from shot location 417 are shown.

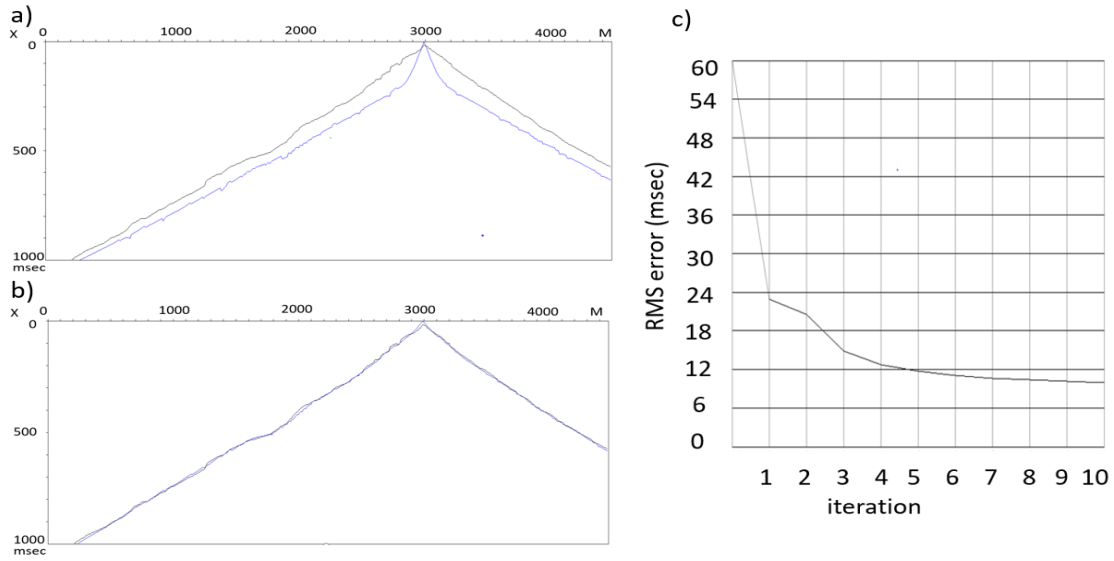

Figure 14. a) Actual first arrival times from shot location plotted in black, minimum travel times from starting model plotted in blue, b) Minimum travel times from velocity model after 10 iterations, c) RMS error at each iteration.

Figure 15 compares the CDP stacks with datum statics correction only and with tomographic weathering statics correction. The images from the tomographic weathering statics corrected CDP stack is more coherent and better resolved than the datum statics corrected CDP stack. These results demonstrate that fast marching method is accurate and is effective when used in refraction tomography.

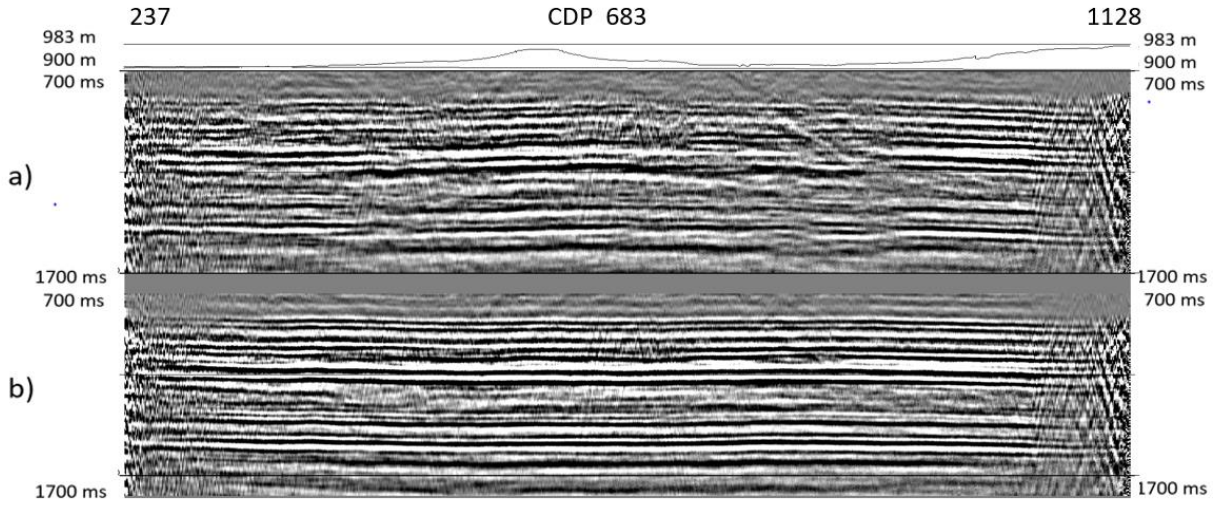

Figure 15. (a) CDP stack with datum statics correction, (b) CDP stack with tomographic weathering statics correction.

CONCLUSION

Fast marching, WFC and paraxial method are all based on the principles of high frequency ray theory; and they all produce accurate travel times when the velocity model varies smoothly. Similar to the classical ray shooting method, paraxial method has the problem of diverging ray paths and shadow zones in area of complex structure. WFC alleviates this problem by interpolating additional ray segments along wavefronts to ensure sufficient ray density. Both paraxial and WFC methods can produce multi-arrivals as well as amplitude; by comparison, the fast marching method can only produce minimum traveltime values. Therefore, WFC and paraxial methods are better suited for depth imaging of complex structures. The fast marching method expands the wavefront and computes traveltime from source to each grid cell without additional interpolation by solving the eikonal equation. Both fast marching and WFC methods can handle up turning rays; therefore, they can be used in refraction tomography. We used the fast marching method in the refraction tomography processing of the Hussar 2D lines. The CDP stack image from the refraction tomography processing is more coherent and better resolved than the CDP stack with datum statics correction. Therefore, refraction travel times computed from fast marching method are accurate and the velocity model from the refraction tomography is reliable and can potentially be used as starting model for full waveform inversion and depth imaging. We did not perform comprehensive analysis of the effects of these ray tracing methods in depth imaging. However, based on the observed geometry of the ray paths in our tests using the Marmousi model, we believe proper application of the multi-value traveltime, amplitude and ray path distance information from WFC and paraxial method can have significant impact on the quality of the final depth image.

REFERENCES

Beydoun,W.B. and Keho,T,H.,1987. The paraxial ray method. ***Geophysics 52***,1639-53.

Cerveny,V., and Hron,F.,1980. The ray series method and dynamic ray tracing system for three-dimensional inhomogeneous media ***Bull.Seismol.Soc.Am. 70***,47-77

Krebes,E.,2010. Theoretical Seismology Lecture Notes. University of Calgary.

Matsuoka,T., and Ezaka, T.,1992. Ray tracing using reciprocity. ***Geophysics 57***,326-33.

Osher,S.,and Sethian,J.A.,1988. Fronts propagation with curvature dependent speed: Algorithms bbased on Hamilton-Jacobi formulation:***J.Computational Phys***.,79,12-49.

Qin,F., Luo.Y., Olsen,K.B., Cai,W., and Schuster,G.T. 1992. Finite difference solution of the eikonal equation along expanding wavefronts. ***Geophysics 57***,478-87.

Rouy,E., and Tourin,A., 1992. A viscosity solution approach to shape-from-shading. ***SIAM J. Num. Anal 29***,867-884.

Sethian,J. and Popovici,A.,1999. 3-D traveltime computation using the fast marching method. ***Geophysics 65***,516-523

Vidale,J.E.,1988. Finite difference calculation of travel times. ***Bull.Seismol.Soc.Am.78***, 2062-76.

Vidale,J.E.,1990. Finite difference calculation of travel times in three dimension. ***Geophysics 55***,521-6

Vinje,V.,Iversen,E.,and Gjoystdal,H.,1993. Traveltime and amplitude estimation using wavefront construction. ***Geophysics 58***,1157-1166